Optics Letters

Mid-IR broadband supercontinuum generation from a suspended silicon waveguide

Rai Kou,[1,4,*] Taiki Hatakeyama,[2] Jason Horng,[1] Ji-Hun Kang,[1] Yuan Wang,[2,4] Xiang Zhang,[2,3,5] and Feng Wang[1,3,6]

[1]Department of Physics, University of California at Berkeley, Berkeley, California 94720, USA
[2]Nanoscale Science and Engineering Center, University of California, Berkeley, California 94720, USA
[3]Materials Sciences Division, Lawrence Berkeley National Laboratory, Berkeley, California 94720, USA
[4]Currently at National Institute of Advanced Industrial Science and Technology (AIST), Tsukuba, Ibaraki, 305-8569, Japan
[5]e-mail: xiang@berkeley.edu
[6]e-mail: fengwang76@berkeley.edu
*Corresponding author: rai.kou-takahashi@aist.go.jp

Received 14 December 2017; revised 13 February 2018; accepted 14 February 2018; posted 16 February 2018 (Doc. ID 315728); published 14 March 2018

Mid-infrared light provides numerous unexpected opportunities in scientific discoveries because this wavelength region covers the fingerprints of various molecular vibrational resonances. However, the light generation efficiency and bandwidth have been a long-standing bottleneck which has limited the development so far. Moreover, the light source that can be integrated with other components such as wavelength filters, detectors, and electronics, will be the key factor toward the future practical applications. Here, we propose an all-air-cladding silicon-rib waveguide to experimentally reveal the nonlinear performance of supercontinuum generation. By tuning the waveguide dispersion parameters with simulation, a continuous broad spectrum of 1.32 octave (2–5 μm) was observed with a pump pulse wavelength of 4 μm. To further investigate our device characteristics, multiple conditions were set by varying the interaction length, pump power, and waveguide dimension, which revealed the nonlinear phenomenon in the waveguide.

OCIS codes: (190.4360) Nonlinear optics, devices; (320.6629) Supercontinuum generation; (130.3060) Infrared.

https://doi.org/10.1364/OL.43.001387

Silicon, a promising electronic material for more than half a century, has recently gained importance as an optical material. As predicted by Soref in his Si-based optoelectronic integrated circuit prediction [1], this material with germanium has been attracting attention in "silicon photonics" since the beginning of this century. The distinctive features of a complementary metal oxide semiconductor (CMOS)-compatible process opened a new world of high-performance optoelectronic circuits with extremely low fabrication cost. However, most applications have been developed for near-infrared (IR) telecommunication bands around an optical wavelength of 1.5 μm so far, even though this material has an excellent transparency window over IR and terahertz bands [2–4]. If a broadband supercontinuum (SC) light source can be generated in such an integrated optical circuit, it will be able to open up possibilities for various applications such as environmental measurement [5], bio-chemical sensing [6], metrology [7], optical communication [8], and absorption spectroscopy in basic science [9]. Furthermore, recent advanced technology of chalcogenide glass-based fibers [10,11] and waveguides [12] generate SC lights very efficiently and broadly, but the future compatibility with electronics integration is still difficult. Previous challenges of the SC light generation from the group IV materials began at a 1.5 μm pump with a standard silicon wire waveguide [13,14], and then gradually extended to a longer wavelength up to a mid-infrared (mid-IR) regime recently. Thanks to the material nature of silicon, the large optical linear susceptibility allows a tight guiding-mode confinement as small as a sub-μm^2 cross-sectional area, and the remarkably large third-order nonlinear susceptibility enables an efficient SC light generation induced by multi-complex light-matter interactions such as self-phase modulation (SPM), cross-phase modulation, four-wave mixing, self-steepening, stimulated Raman scattering (SRS), Cherenkov radiation, and soliton fission. It should be noted that the Kerr coefficient $n_{2,Si}$ in bulk crystalline silicon has been reported as 4.2×10^{-18} m^2/W [15,16] which is about 20 times larger in value than silicon nitride [17], and more than 160 times larger than silica glass [18] around a wavelength of 1.5 μm. Moreover, a highly confined waveguide due to silicon's high refractive index allows large anomalous dispersion that can maintain a very short pulse duration by counterbalancing the SPM effect. Such a dispersion-induced pulse compression effect, which can be realized by tuning the waveguide dimensions, creates strong peak power and leads to efficient SC generation. Reducing multi-photon absorption is also a remarkable advantage when moving the wavelength range of interest to the mid-IR region. While the Kerr coefficient $n_{2,Si}$ does not change by orders of magnitude as the wavelength becomes longer, the multi-photon

absorption such as two-photon absorption and three-photon absorption can be greatly suppressed [19–21].

According to the latest updates related to the SC generation in mid-IR, an octave-spanning SC light ranging from 1.5 to 3.6 μm [22] and a frequency comb ranging from 1.5 to 3.2 μm [23] using a standard silicon-channel waveguide have been demonstrated. The limited spectral performance is restricted by the strong absorption edge due to a Si-O-Si vibrational mode from around 2 μm (e.g., absorption index k reaches $\sim 10^{-4}$ at 4 μm and $\sim 10^{-2}$ at 5 μm) and the presence of OH groups at wavelengths of 2.73–2.85, 3.5, and 4.3 μm [24]. (Note that the absorption rate depends greatly on the sample preparation methods.) In another report, over 1.5 octave SC spectrum covering from 2.0 to 5.6 μm with a silicon-on-sapphire platform [25] has been achieved. Although the sapphire cladding has a wider transparent window compared to silicon dioxide, the absorption coefficient is continuously rising beyond 5 μm [26]. To overcome these restrictions, we demonstrate a suspended all-air-cladding silicon waveguide to generate SC light in the mid-IR range. This structure no longer requires a special wafer-bonding process that causes a cost increase and incompatibility with the standard CMOS process. In fact, several groups have predicted an efficient SC generation from any suspended Si, Ge, or SiGe waveguides by theoretical analysis [25,27,28], but the experimental demonstration has not been reported. According to the past research, several different types of transparent silicon waveguides have been proposed for the mid-IR wavelength such as a suspended structure fabricated by wafer boding [29] or wet etching [30], and low-loss platform enabled by mode-distribution adjustment [31]. In this Letter, we selected the wet etching method because of the design flexibility of the waveguide dimension, as well as wavelength dispersion and relatively simple fabrication procedures.

Figure 1(a) shows the schematic illustration of the suspended waveguide. The thicknesses of the waveguide (H), slab (S), and buried oxide were 2 μm, 500 nm, and 3 μm, respectively. There were 1 μm × 2 μm holes around the waveguide for wet etching. The distance between the waveguide and the hole was 4 μm. The waveguide was fabricated on a SOI substrate. The device layer was grown by the floating-zone method to minimize free carrier absorption. The pattern was written by an e-beam lithography machine and transferred to the substrate by reactive ion etching (RIE). The holes around the waveguide were made by e-beam lithography and RIE processes. After making the holes, the substrate was dipped in 5∶1 buffered hydrofluoric acid (BHF) to remove the oxide layer below the waveguide. Figure 1(b) shows a cross-sectional image of the suspended silicon waveguide. The silicon membrane does not have a deflection because the slab is thick enough to avoid the mechanical instability. If the thickness of slab is less than 500 nm, the suspended waveguide would bend down to the substrate. The deflection of the beam at the center point is described by $Fl^3/4ES^3$, where F is the force on the center of the beam, and l is the length of the beam between the supports. E represents Young's modulus of silicon. Given that the force is applied only by the weight of the waveguide, the maximum deflection by the force is less than 1 nm. Therefore, the deflection by the weight of the waveguide is negligible. The deflection of the membrane is also caused by the residual stress in the silicon layer. The deflection induced by the residual stress is written by $3Ml^2/4ES^3$, where M is the bending moment. Thus, the deflection by the residual stress is proportional to S^{-3}. This trend has been experimentally shown in a previous report [20]. It indicates that the thicker membrane has more mechanical stability if the residual stress does not change. Besides, Young's modulus of a silicon membrane becomes lower than the bulk silicon when the thickness of the membrane is less than 300 nm [21]. For example, Young's modulus of a 300 nm thick silicon cantilever is 168 GPa, which is the same as the bulk silicon, while Young's modulus of a 12 nm thick silicon cantilever is 53 GPa. By considering the residual stress and Young's modulus of a silicon membrane, we conclude that our device is mechanically stable compared to thin silicon membranes (<300 nm).

A flat dispersion in an anomalous regime results in group-velocity-matched light propagation in a short pulse width by balancing with the SPM effect. We calculated the dispersion curves for a single mode and tightly confined the rib waveguides with W:1000–3000 nm × H:500 nm × S:100 nm [Fig. 2(a)]. While the anomalous dispersion reaches up to 900 ps/nm/km at the narrowest waveguide width (W: 1000 nm), the available bandwidth was limited due to the mode confinement. (Note that the positive value in the vertical axis corresponds to the

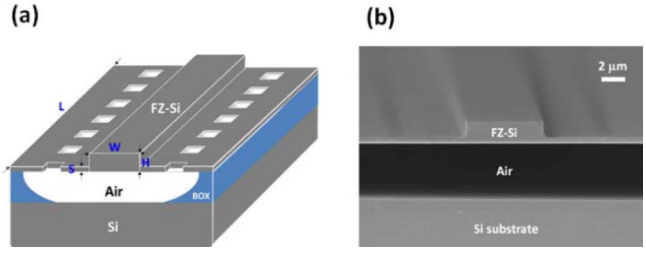

Fig. 1. (a) Schematic of suspended silicon waveguide. (b) Scanning electron microscope image of the suspended waveguide.

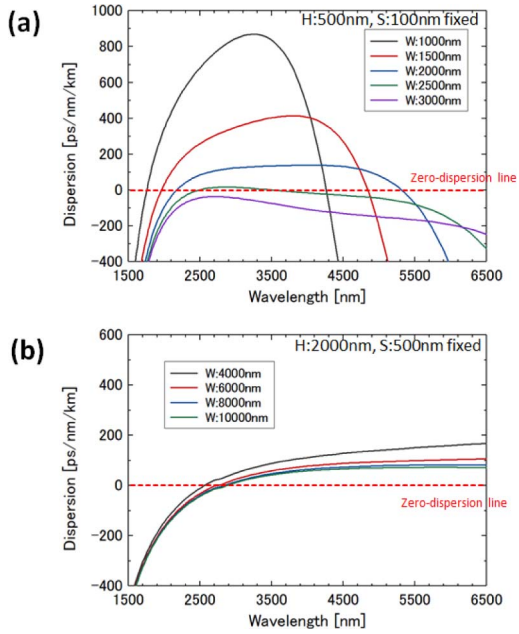

Fig. 2. Calculated dispersion profiles to compare the difference between thin and thick SOI substrates. (a) With a thin SOI thickness (H) of 500 nm and slab thickness (S) of 100 nm. (b) With a thick SOI thickness (H) of 2000 nm and a slab thickness (S) of 500 nm.

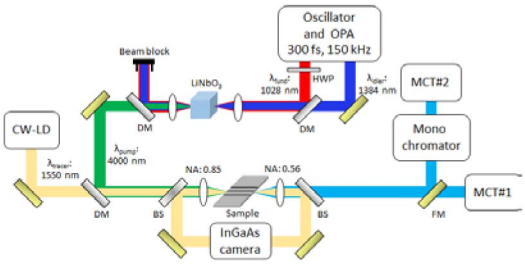

Fig. 3. Schematic of the experiment setup. HWP, half-wave plate; DM, dichroic mirror; FM, flip mirror; BS, beam splitter.

anomalous dispersion.) Additionally, both the dispersion and bandwidth are significantly modulated by the dimensions of the core, which results in a low tolerance to the fabrication error. In Fig. 2(b), we designed a relatively large-core waveguide with dimensions of W:4000–10000 nm × H:2000 nm × S:500 nm to improve the dispersion profiles to be wider and flatter over the mid-IR region. When the thickness of the waveguide is 2000 nm, the dispersion is not greatly modulated by varying the width of the waveguide. Thus, our device is not affected by the fabrication errors compared to the thinner waveguides. To realize an efficient light coupling, 10 μm wide adiabatic tapers were equipped at both input and output edges.

The experiment setup for SC generation is illustrated in Fig. 3. A pump light source is generated by a Yb:KGW pulse laser system followed by an optical parametric amplifier. The oscillator produces a 300 fs short pulse with a center wavelength of 1028 nm at a repetition rate of 150 kHz. By adjusting the $LiNbO_3$ crystal angle for a birefringent phase-matched condition between the fundamental (λ_{fund}:1028 nm) and idler (λ_{idler}:1384 nm) beams, a difference-frequency generation wavelength as a pump source (λ_{pump}:4000 nm) is generated. The light polarization is adjusted to a quasi-TE mode (parallel to substrate). The femtosecond mid-IR pump pulse is coupled into the suspended silicon waveguide by using a pair of high-numerical-aperture (NA = 0.85 at input, 0.56 at output) black-diamond (BD) lenses with an anti-reflection coating for the 3–5 μm range. To couple the pump light efficiently, a continuous-wave (CW) laser diode (λ_{tracer}: ~ 1500 nm) was used for imaging the input/output cross sections of the waveguide by an InGaAs camera, as well as tracing of the mid-IR light path. For the sample position alignment, a liquid-nitrogen-cooled HgCdTe detector (MCT#1) coupled the output light directly followed by a current-mode transimpedance preamplifier and a lock-in amplifier. Next, a refractive-grating-based (300 grooves/mm, 2–5 μm design wavelength) monochromator with an MCT#2 was used to perform the spectroscopy in 20 nm resolution steps.

We start the device characterization with loss measurement by coupling a CW-LD tracer light. With a waveguide width (W) of 8 μm, a transmittance of 15–20% using two coupling lenses was measured across a 12 mm long device. Next, we measured the loss at the pump wavelength of 4 μm. The coupling efficiency at the input was estimated to be ~15%. The loss contains the transmittance of a BD lens (50%), Fresnel reflection on the silicon surface, and mode-field mismatching between the incident light and confinement mode (especially due to the waveguide height). The propagation loss was ~5 dB/cm at the pump wavelength. Taking the maximum input pump intensity of 28.8 mW for an example, the actual coupled power to the waveguide is around 4.3 mW which corresponds to 96 kW in peak power and 600 GW/cm^2 in power density. To prevent launching any higher-order modes coupling we optimized the mode-field distribution to be single by monitoring it with an InGaAs camera from the output. At the beginning of the alignment for SC generation, we used neutral density (ND) filters to attenuate the pump intensity to operate at sub milliwatt level to protect the device surface from excessive heat. Then the focusing position was aligned by iterations to maximize the light transmittance from the wavelength of 1.5–4 μm. Figure 4(a) shows the spectra obtained using three input intensity conditions of 1.9, 14.9, and 28.6 mW (average power), with a 7 mm long device. At the maximum input power, a spectrum ranging 3.0–4.7 μm was observed at an output intensity of −30 dB level. A simple mountain-shaped spectrum suggests that the SPM effect is a dominant nonlinearity that spreads toward both sides while increasing the pump power. (Note that the sharp absorption observed at around 4.25 μm was caused by a vibration of asymmetric-bond stretching in CO_2.) According to Ref. [13], the SRS plays a small role in a crystalline-silicon waveguide because the gain bandwidth is narrow enough. Next, a 12 mm long device was measured to investigate the interaction length dependence. Figure 4(b) exhibits the spectra measured with comparable pump intensity from 1.5 to 28.8 mW. Now, we recognized that even with the 1.5 mW, the pumped spectrum induced spectral broadening slightly. As we increase the pump intensity above 10 mW, many small peaks were induced due to the soliton fission, which means different nonlinear broadening mechanisms were observed at the device lengths of 7 and 12 mm. According to the Ref. [32], the dispersion length L_D ($= T_0^2/|\beta_2|$) is ~100 mm with $T_0 = 300$ fs, and $\beta_2 = -0.85$ ps^2/m at 4 μm. The soliton fission point can usually be observed in the range of 10–50% of

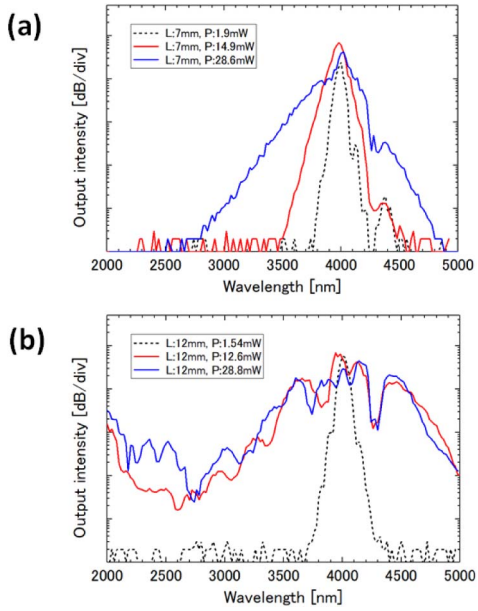

Fig. 4. (a) Measured spectra with a 7 mm long device. The average pumping power was at 1.9, 14.9, and 28.5 mW. (b) With a 12 mm long device, the average pumping power was at 1.5, 12.6, and 28.8 mW.

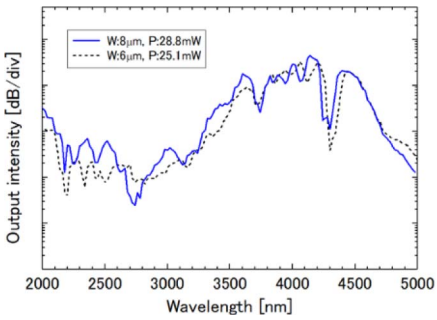

Fig. 5. Measured spectra with two different waveguide widths (W) of 6 and 8 μm. The input pumping powers were set to be over 25 mW.

L_D that approximately agrees with our measurement result. The soliton order is estimated to be 48 at the input power of 10 mW. On the other hand, the spectrum distributions of 12.6 and 28.8 mW were almost identical over a wide range because of their approach toward the saturation regime, as well as the damage threshold of silicon. This saturation sign suggested that nonlinear absorption effects such as the four-photon absorption-induced free-carrier absorption, possibly occurred in our waveguide between the 7 to 12 mm interaction length. We note that the light intensity gradually becomes weaker beyond the wavelength of 4.5 μm independent of the pump intensity, although the wide anomalous dispersion shown in Fig. 2(b) indicates that the suspended silicon waveguide can support a broad SC extending to a much longer wavelength. Apparently, there are additional losses in the silicon waveguide present at long wavelengths. The microscopic origin of this extra loss mechanism is not known yet, and further systematic studies will be required to realize the full potential of the suspended silicon waveguide structures. Finally, we measured a device with a center waveguide width (W) of 6 μm, as shown in Fig. 5. Similar trends were found over the full range, using the same input power.

In conclusion, a silicon-based broadband mid-IR white light source is experimentally demonstrated. While conventional silicon-photonic devices have a strong light absorption beyond 4 μm induced by the surrounding SiO_2 cladding, we improved this critical restriction with a fully suspended silicon waveguide structure. With pumping power >10 mW, we obtained an SC spectrum range from 2 to 5 μm. We expect this experimental demonstration with the suspended waveguide has paved the way for further development of mid- and far-IR SC generation.

Funding. U.S. Department of Energy (DOE), Office of Science (SC), Basic Energy Sciences (BES), Materials Sciences and Engineering Division (DE-AC02-05-CH11231, KC12XZ); Japan Society for the Promotion of Science (JSPS).

Acknowledgment. This Letter was primarily supported by the U.S. Department of Energy, Office of Science, Basic Energy Sciences, Materials Sciences and Engineering Division within the Metamaterials Program. R. Kou was supported by JSPS Overseas Research Fellowships Program.

REFERENCES

1. R. A. Soref and J. P. Lorenzo, IEEE J. Quantum Electron. **22**, 873 (1986).
2. D. Grischkowsky, S. Keiding, M. Vanexter, and C. Fattinger, J. Opt. Soc. Am. B **7**, 2006 (1990).
3. J. M. Dai, J. Q. Zhang, W. L. Zhang, and D. Grischkowsky, J. Opt. Soc. Am. B **21**, 1379 (2004).
4. D. Chandler-Horowitz and P. M. Amirtharaj, J. Appl. Phys. **97**, 123526 (2005).
5. L. Tao, K. Sun, M. A. Khan, D. J. Miller, and M. A. Zondlo, Opt. Express **20**, 28106 (2012).
6. M. Sieger and B. Mizaikoff, Anal. Chem. **88**, 5562 (2016).
7. A. Schliesser, N. Picque, and T. W. Hansch, Nat. Photonics **6**, 440 (2012).
8. H. Takara, T. Ohara, T. Yamamoto, H. Masuda, M. Abe, H. Takahashi, and T. Morioka, Electron. Lett. **41**, 270 (2005).
9. K. F. Mak, L. Ju, F. Wang, and T. F. Heinz, Solid State Commun. **152**, 1341 (2012).
10. C. R. Petersen, U. Møller, I. Kubat, B. Zhou, S. Dupont, J. Ramsay, T. Benson, S. Sujecki, N. Abdel-Moneim, Z. Tang, D. Furniss, A. Seddon, and O. Bang, Nat. Photonics **8**, 830 (2014).
11. T. L. Cheng, K. Nagasaka, T. H. Tuan, X. J. Xue, M. Matsumoto, H. Tezuka, T. Suzuki, and Y. Ohishi, Opt. Lett. **41**, 2117 (2016).
12. Y. Yu, X. Gai, P. Ma, K. Vu, Z. Y. Yang, R. P. Wang, D. Y. Choi, S. Madden, and B. Luther-Davies, Opt. Lett. **41**, 958 (2016).
13. L. H. Yin, Q. Lin, and G. P. Agrawal, Opt. Lett. **32**, 391 (2007).
14. Q. Lin, O. J. Painter, and G. P. Agrawal, Opt. Express **15**, 16604 (2007).
15. M. Dinu, F. Quochi, and H. Garcia, Appl. Phys. Lett. **82**, 2954 (2003).
16. Q. Lin, J. Zhang, G. Piredda, R. W. Boyd, P. M. Fauchet, and G. P. Agrawal, Appl. Phys. Lett. **91**, 021111 (2007).
17. K. Ikeda, R. E. Saperstein, N. Alic, and Y. Fainman, Opt. Express **16**, 12987 (2008).
18. K. S. Kim, R. H. Stolen, W. A. Reed, and K. W. Quoi, Opt. Lett. **19**, 257 (1994).
19. F. Gholami, S. Zlatanovic, A. Simic, L. Liu, D. Borlaug, N. Alic, M. P. Nezhad, Y. Fainman, and S. Radic, Appl. Phys. Lett. **99**, 081102 (2011).
20. A. D. Bristow, N. Rotenberg, and H. M. van Driel, Appl. Phys. Lett. **90**, 191104 (2007).
21. M. Dinu, IEEE J. Quantum Electron. **39**, 1498 (2003).
22. R. K. W. Lau, M. R. E. Lamont, A. G. Griffith, Y. Okawachi, M. Lipson, and A. L. Gaeta, Opt. Lett. **39**, 4518 (2014).
23. B. Kuyken, T. Ideguchi, S. Holzner, M. Yan, T. W. Hänsch, J. Van Campenhout, P. Verheyen, S. Coen, F. Leo, R. Baets, G. Roelkens, and N. Picqué, Nat. Commun. **6**, 6310 (2015).
24. R. Kitamura, L. Pilon, and M. Jonasz, Appl. Opt. **46**, 8118 (2007).
25. N. Singh, D. D. Hudson, Y. Yu, C. Grillet, S. D. Jackson, A. Casas-Bedoya, A. Read, P. Atanackovic, S. G. Duvall, S. Palomba, B. Luther-Davies, S. Madden, D. J. Moss, and B. J. Eggleton, Optica **2**, 797 (2015).
26. J. Kischkat, S. Peters, B. Gruska, M. Semtsiv, M. Chashnikova, M. Klinkmuller, O. Fedosenko, S. Machulik, A. Aleksandrova, G. Monastyrskyi, Y. Flores, and W. T. Masselink, Appl. Opt. **51**, 6789 (2012).
27. J. H. Yuan, Z. Kang, F. Li, X. T. Zhang, X. Z. Sang, Q. Wu, B. B. Yan, K. R. Wang, X. Zhou, K. P. Zhong, G. Y. Zhou, C. X. Yu, C. Lu, H. Y. Tam, and P. K. A. Wai, J. Lightwave Technol. **35**, 2994 (2017).
28. M. H. Yang, Y. H. Guo, J. Wang, Z. H. Han, K. Wada, L. C. Kimerling, A. M. Agarwal, J. Michel, G. F. Li, and L. Zhang, Opt. Express **25**, 16116 (2017).
29. J. Chiles, S. Khan, J. Ma, and S. Fathpour, Appl. Phys. Lett. **103**, 151106 (2013).
30. Y. Xia, C. Y. Qiu, X. Z. Zhang, W. L. Gao, J. Shu, and Q. F. Xu, Opt. Lett. **38**, 1122 (2013).
31. S. A. Miller, M. J. Yu, X. C. Ji, A. G. Griffith, J. Cardenas, A. L. Gaeta, and M. Lipson, Optica **4**, 707 (2017).
32. G. P. Agrawal, *Nonlinear Fiber Optics*, 5th ed. (Academic, 2013), Chaps. 3 and 12.